INSTITUTE OF PHYSICS PUBLISHING PLASMA PHYSICS AND CONTROLLED FUSION

Plasma Phys. Control. Fusion **43** (2001) A267–A276 PII: S0741-3335(01)28405-X

Proton imaging: a diagnostic for inertial confinement fusion/fast ignitor studies

M Borghesi[1], A Schiavi[2], D H Campbell[2], M G Haines[2], O Willi[2,7], A J MacKinnon[3], L A Gizzi[4], M Galimberti[4], R J Clarke[5] and H Ruhl[6]

[1] Department of Pure and Applied Physics, The Queen's University of Belfast, Belfast BT7 1NN, UK
[2] The Blackett Laboratory, Imperial College, London SW7 2BZ, UK
[3] Lawrence Livermore National Laboratory, Livermore, CA, USA
[4] Intense Laser Irradiation Laboratory, IFAM, Area della Ricerca – CNR, 56100 Pisa, Italy
[5] Central Laser Facility, Rutherford Appleton Laboratory, Chilton OX11 0QX, UK
[6] Max-Born-Institut,12489 Berlin, Germany

Received 22 June 2001
Published 22 November 2001
Online at stacks.iop.org/PPCF/43/A267

Abstract

Proton imaging is a recently proposed technique for diagnosis of dense plasmas, which favourably exploits the properties of protons produced by high-intensity laser–matter interaction. The technique allows the distribution of electric fields in plasmas and around laser-irradiated targets to be explored for the first time with high temporal and spatial resolution. This leads to the possibility of investigating as yet unexplored physical issues. In particular we will present measurements of transient electric fields in laser–plasmas and around laser-irradiated targets under various interaction conditions. Complex electric field structures have been observed in long-scale laser-produced plasmas, while global target charge-up and growth of electromagnetic instabilities have been detected following ultraintense interactions with solid targets.

1. Introduction

During the interaction of ultraintense laser pulses with plasmas and solid targets, a considerable fraction of the laser energy is deposited into highly energetic charged particles. One of the most exciting results recently obtained in this area of research is the observation of very energetic beams of protons, generated during the interaction of ultraintense short pulses with solid targets. In a number of experiments, performed with different laser systems and in different interaction conditions, protons with energies up to several tens of MeV have been detected behind thin foils irradiated with high-intensity pulses [1–3]. In these experiments it was seen that the particle beams are directed along the normal to the back surface of the target, and have a small angular aperture at the highest energies. As proton beams are observed even using targets

[7] Present address: Institut für Laser- und Plasmaphysik, Heinrich-Heine-Universität, Düsseldorf, Germany

which nominally do not contain hydrogen, protons are thought to originate from hydrocarbon impurities located on the target surfaces [4] or from bulk contamination of the target. Proposed theoretical models indicate that the protons gain their energy from the enormous electric field (∼MV/micron) set up by laser-accelerated fast electrons via space-charge at the back target surface [5]. As protons are easier to accelerate than heavier ions, protons will be the dominant component of the ion emission [6, 7].

The particular properties of the proton beams (small source size, high degree of collimation, short duration, energy dependence on the target characteristics) make them of particular interest in view of possible applications. Among these, their use as the ignition trigger in the fast ignitor scheme has been proposed [8]. The characteristics of the proton beam make it very suitable for applications as a probe in high-density matter investigations. As a matter of fact, the use of protons as a radiographic source is an idea which has circulated for many years [9]. Applications of proton radiography have been proposed in the biomedical area [10] or in testing of thick systems [11]. Linear or cyclotron accelerators are used to obtain the proton energies required for these applications. Laser-produced proton beams represent a feasible alternative with enormous potential when high spatial/temporal resolution is required.

A particularly interesting application of laser-produced proton beams is the detection of electric and magnetic fields generated during the interaction of intense laser pulses with high-density plasmas. In this context, *proton imaging* can be developed as a diagnostic with great potential for inertial confinement fusion (ICF) studies. For example, the possibility of accessing directly electric field distributions in dense plasmas may shed new light on issues as hydrodynamic and electromagnetic instabilities highly detrimental for ICF. The technique has great potential for access to the complex and yet unexplored electric and magnetic field distributions in indirect drive target assemblies [12]. In a fast ignitor context, it will contribute to the study of the large transient electric and magnetic fields generated in high-intensity laser–matter interactions. The magnitude and characteristics of these fields are currently the subject of much conjecture in the short-pulse, high-intensity plasma physics community.

In this paper the results of a series of experiments performed at the Rutherford Appleton Laboratory will be presented and discussed, in which the proton source has been applied for the first time as a particle probe in a range of laser–plasma interaction conditions.

2. Experimental set-up

The Vulcan Nd : glass laser [13] operating in the chirped pulse amplification (CPA) mode was used in the experiment. The main targets (used for the production of the proton beams) were Al foils, 1–2 mm wide and 3–25 μm thick. The 1.054 μm CPA interaction pulse, 1 ps in duration, with energy up to 100 J was focused by an $f/3.5$ off-axis parabola (OAP) onto the centre of the main target. The incidence was about 15° off normal. There was the possibility, exploited in the final part of the experimental campaign, of splitting the main CPA pulse into two separate high-intensity pulses, and to focus them employing two separate $f/3.5$ OAPs. The focal spot varied between 8 and 10 μm diameter at full width at half maximum (FWHM), containing 30–40% of the energy, and giving intensities up to $5–7 \times 10^{19}$ W cm^{-2}. Heating pulses with duration 0.5–1 ns were also available, and were used to provide, in some parts of the experiment, intensities on target in the range 10^{13}–10^{15} W cm^{-2}. A low-energy fraction of the main CPA pulse was frequency quadrupled and used as a transverse optical probe pulse.

A summary description of the beam arrangements used in the various experimental tests performed will be given at the beginning of each experimental section. The detector employed in the whole campaign consisted of a stack of several layers of radiochromic (RC) film. As shown in figure 1(*a*), the film consists of 270 μm thick plastic containing a double layer of

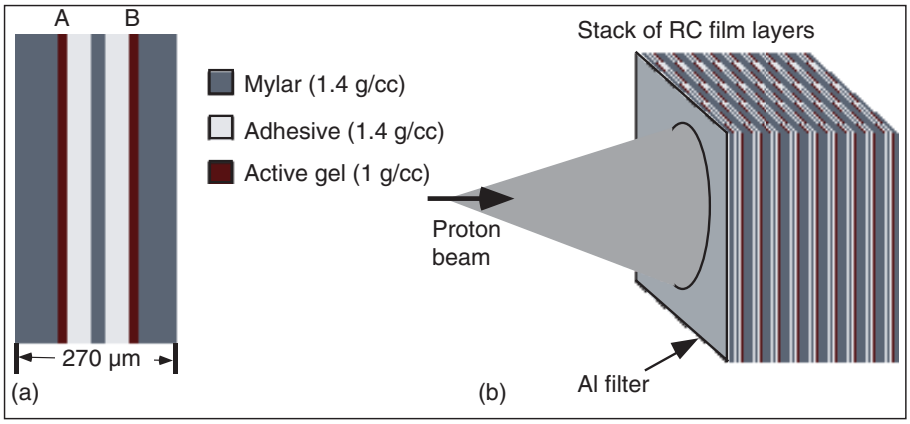

Figure 1. Schematic of (*a*) a layer of RC film; (*b*) set-up for spectrally resolved proton beam detection.

organic dye, which reacts to ionizing radiation [14]. The equivalent dose of energetic protons stopped in the film can be measured from the changes in optical density undergone by the film, yielding information on the number and energy of the protons. By using them in a stack, each layer of film acts as a filter for the following layers. Since protons deposit energy mainly in the Bragg peak at the end of their range, each RC film layer spectrally selects a narrow range of proton energies. Plastic track detectors [15] were also used in some occasions to confirm that the structures observed were due to protons and not to electrons or x-rays to which the RC film is also sensitive. Al filters (25–50 μm) were placed in front of the first layer of film giving a minimum detectable proton energy of about 3 MeV. Al and C ions from the target are stopped by the Al filter and the first RC layer and do not contribute to the signal observed in the successive layers [1].

3. Proton beams and proton imaging

The laser-produced proton beam was characterized in view of its application as a particle beam probe. The protons were produced by focusing the CPA pulse onto the Al foil, and detected by placing the RC film stack at the back of the target, typically at a distance of about 2 cm. It was found that the proton beams have high brightness, typically with 10^{12} protons with energy above 3 MeV per shot (at a laser irradiance of the order of 5×10^{19} W cm^{-2}). As observed in previous experiments, the beams were highly directional, propagating along the normal to the back surface of the target with small angular divergence (about 15° for 10 MeV protons). The response of each RCF layer to high-energy protons has been determined using Monte Carlo modelling of the deposited energy by the particles. A strong proton signal was observed out to the layer corresponding to proton energy just above 20 MeV. The energy deposited within each film layer can be extracted from the absolutely calibrated film. By doing this for each film layer and fitting an exponential energy spectrum, an estimate of the proton energy spectrum and total energy can be extracted from the film data [16]. The mean proton energy of the exponential fit is 3.75 ± 0.3 MeV with a total energy of 2.2 J in an equivalent Maxwellian with a temperature of 2.5 MeV. During the experiments the source size of the proton beam was estimated using a penumbral edge method, setting an upper limit of 15–20 μm diameter for the source of 10 MeV protons.

As should be clear, there are several reasons which make laser-produced proton beams very interesting for probing applications. Among these are: the small source size, leading to high spatial resolution in imaging applications; the short pulse duration, measured to be a few ps in our conditions; the low divergence and high brightness of the beam; and the long stopping range of 10–30 MeV protons, i.e. the possibility of penetrating reasonably thick objects. In addition, high spatial and spectral resolution is guaranteed by an appropriate choice of detector (e.g. RCF stacks), and the proton beam characteristics can be tuned by suitably changing the laser and target parameters. The temporal resolution obtainable with these beams is far beyond the possibilities of beams provided by conventional accelerators. Further, as will be seen in the following sections, the fact that the beams are not monochromatic is far from being a disadvantage for the proposed applications. Finally their ease of use and synchronization is a clear advantage in laser–plasma and inertial confinement fusion related experiments; the fact that, being charged, they can be used for diagnosing electric and magnetic fields makes proton beam probing an interesting alternative to more established techniques as x-ray probing.

Due to the small size of the source, we were able to implement a scheme of point projection imaging, with the object placed between the proton source (i.e. the back side of the primary target) and the detector. The magnification of the image was simply determined by the ratio of the detector-to-object and object-to-source distances. In general, the intensity distribution cross-section of the proton beam is modified both by collisional stopping/scattering, and by deflections due to electric and magnetic fields. However, as will be seen in the following sections, significant changes in the proton beam were even observed in underdense plasmas and very thin targets, where collisional stopping of the multi-MeV protons could be excluded since the aerial density of the target was orders of magnitude smaller than the stopping range for the protons used. Under these conditions, proton imaging appears as a powerful and unique technique for the direct detection of electric and magnetic fields distribution in laser-irradiated targets and plasmas. Depending on the target and irradiation geometry employed, it can be made more sensitive to the detection of electric rather than magnetic fields. Three-dimensional particle-in-cell simulations performed by Dr H Ruhl (MBI-Berlin) have studied the propagation of proton beams through plasmas, [17] and have confirmed that electric fields structures present in the plasma (as for example those associated with small-scale density non-uniformities) can indeed be imprinted on the proton beam intensity profile.

4. Imaging of cold solid objects

When thick solid obstacles were placed in the beam, a shadow of the object was observed in the proton beam due to collisional stopping in the target. However, as mentioned above, a shadow was observed even when objects with a thickness much smaller than the proton penetration depth were used, e.g. a mesh formed by 10 μm Cu wires with 25 μm spacing, or by 25 μm Cu wires with 100 μm spacing. The set-up for this particular test is depicted in figure 2(*a*). The mesh was parallel to the main target, i.e. perpendicular to the proton beam. The distance between the proton source and the mesh was 1 mm, while the first of the radiochromic film layers was positioned at 22 mm from the source.

A shadow of the mesh was observed on the radiochromic film, as shown in figure 2(*b*). The image shown in the picture has been obtained with 15 MeV protons and the 25 μm spacing mesh. The shadow of the wires can be observed clearly, the contrast of the picture being quite sharp. Figure 2(*c*) shows the optical density lineout across the shadow of a mesh with 100 μm spacing, obtained with 20 MeV protons. The optical density modulation observed is of the order of 0.2. It should be recalled that the stopping range of 20 MeV protons in Cu is about 800 μm, and the collisional energy loss for such energetic protons in 25 μm of

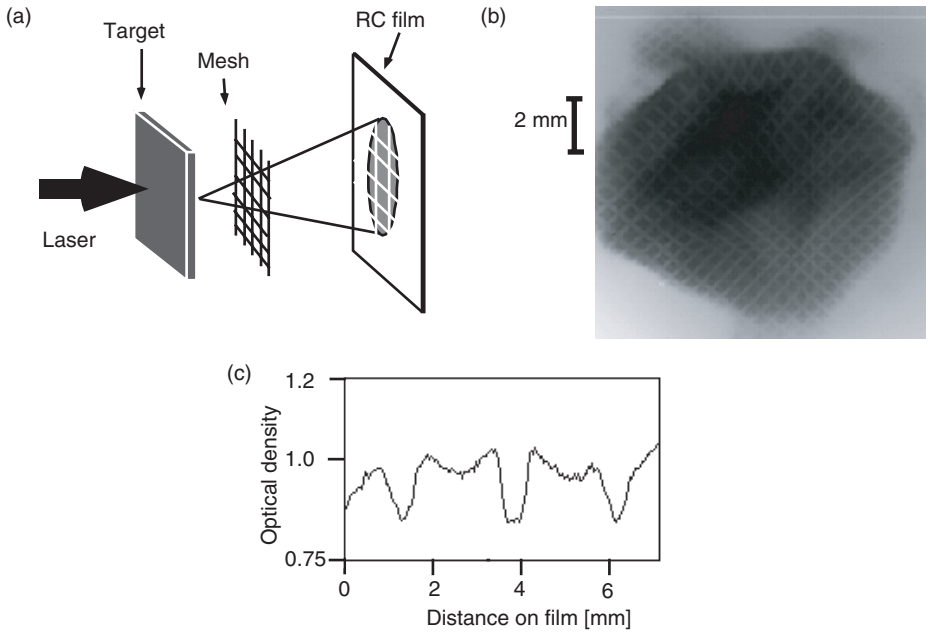

Figure 2. (*a*) Set-up for proton imaging of a mesh. (*b*) Image of a mesh with 25 μm spacing (10 μm Cu wires) obtained with 15 MeV protons. (*c*) Lineout across image of a mesh with 100 μm spacing (25 μm Cu wires) obtained with 20 MeV protons.

Cu is just $\Delta E/E \sim 2 \times 10^{-4}$. Such a variation is too small to produce any detectable effect on our diagnostic. Under these conditions scattering is also unimportant; therefore the shadow observed must be due to some different effect. Our present explanation is that the mesh charges up positively, due, for example, to hot electrons preceding the proton beam and expelling cold electrons from the target. The deflection of the protons due to the electric field in the proximity of the wires is then responsible for the creation of the mesh shadow on the detector, where pile-up of the deflected protons is observed beside the regions of minimum transmission. An estimate of the linear charge on the mesh can be obtained via particle tracing, giving $\lambda \sim 10^{-6}\,\mathrm{C\,m^{-1}}$.

5. Imaging of laser-produced plasmas

The sensitivity of the proton beam to electric fields, demonstrated in the measurements reported in the previous section, makes proton imaging a valid and unique diagnostic for investigating electric field distributions inside plasmas. The diagnostic potential of this application was tested in part of our experimental campaign. A preformed plasma was created by irradiating a secondary target with 600 ps, 0.527 μm heating pulses, prior to the CPA pulse interaction with the primary target. The experimental set-up for this part of the experiment is shown in figure 3. As shown in the figure, both *face-on* and *side-on* geometry was used. When using face-on geometry, transverse optical probing of the preformed plasma could also be performed. The proton beam was produced as usual from a 25 μm Al foil, and the secondary target also consisted of a 25 μm Al foil. The heating irradiance on target varied between 5×10^{13} and $10^{15}\,\mathrm{W\,cm^{-2}}$, with typical delays between the plasma formation and the CPA interaction with the primary target in the range 200–800 ps. When no preformed plasma was

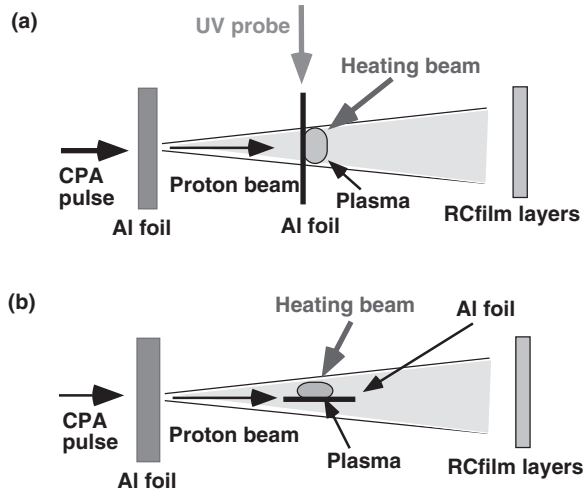

Figure 3. Set-up for proton imaging of plasmas: (*a*) face-on set-up; (*b*) side-on set-up.

produced onto the secondary Al foil, the proton beam was, as expected, unperturbed, except for some charging-up-induced deflection at the edge of the foil. When the secondary foil was laser-heated the situation changed, and, under certain conditions, the presence of the plasma perturbed significantly the intensity distribution of the proton beam.

Most importantly, the perturbations imposed on the intensity profile of the proton beam appeared to depend strongly on the plasma conditions. As a matter of fact, changing the irradiation parameters led to striking differences in the modulation pattern superimposed onto the proton beam. An example of this is given in figure 4, where the RC film images pertaining to different irradiation conditions are shown. The structures observed differ markedly between the case in which no beam smoothing is applied to the beam, and the case in which phase zone plates (PZP) [18], producing an ordered hot spot structure in the focal spot profile, are employed. In particular, side-on images indicate clearly the presence of chaotic structures in the former case, while a regular pattern is observed in the latter. In all cases these structures were only observed within the duration of the heating pulse, and disappeared at later times. We believe that these structures are imprinted by electric fields present inside the plasma, which are strictly related to the laser intensity distribution. Detailed analysis and modelling is ongoing.

6. Imaging of ultraintense interactions

In part of the experimental campaign, proton imaging was applied to the study of ultraintense laser–plasma interactions. These measurements took advantage of the unique possibility of employing two temporally and spatially independent high-power CPA pulses. The second pulse (CPA_2) was split off the main pulse (CPA_1) before amplification. Due to set-up constraints, the energy content of each pulse was about 20 J, focusable to intensities in the range $0.5–1.0 \times 10^{19}$ W cm^2. The temporal separation of the two pulses could be varied shot-to-shot. The two beams were focused from different directions, as shown in figure 5(*a*), with separate $f/3.5$ optics. The CPA_2 pulse was used to produce a proton beam from an Al foil, and the proton beam was used to probe the interaction of the CPA_1 pulse with solid targets.

It should be noted here that, when probing an object undergoing fast changes, the fact that the proton beams are not monochromatic is actually an advantage, as it can be exploited to

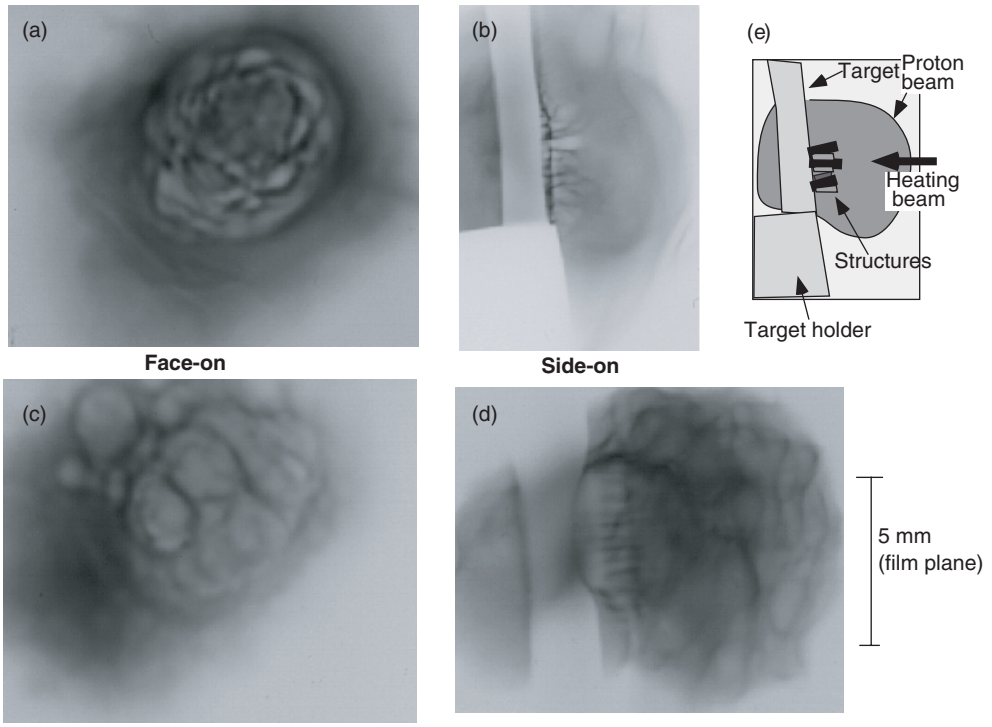

Figure 4. Face-on and side-on proton images of plasmas produced by laser irradiation of 25 µm foils (*a*, *b*) Heating focal spot: 100 µm diameter with no beam smoothing; irradiance: $I \sim 5 \times 10^{14}$ W cm^2. (*c*, *d*) Heating focal spot: 250 µm diameter with beam smoothing (phase zone plates) $I \sim 10^4$ W cm^2. (*e*) Schematic showing the main characteristics of the side-on images.

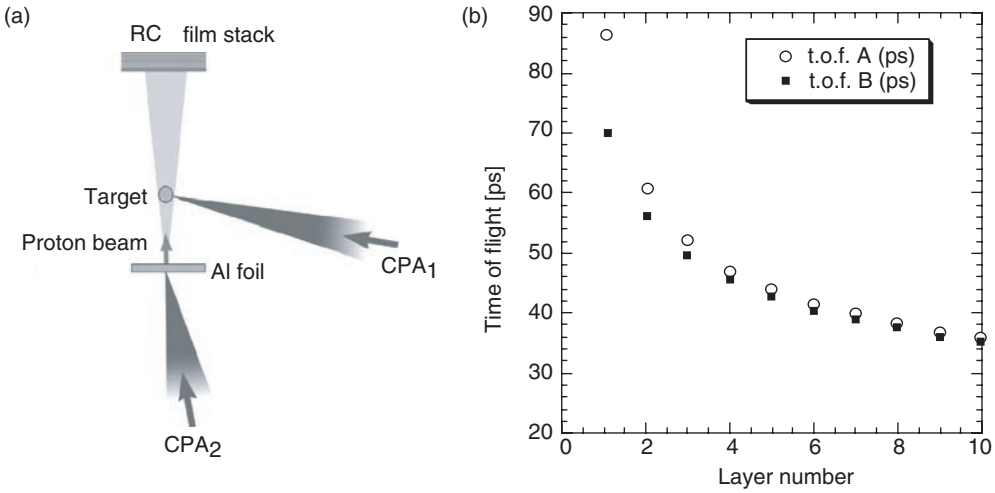

Figure 5. (*a*) Set-up for proton imaging of ultraintense interactions. Typically the distance between the proton source and the main target was 2 mm, and the detector was about 2 cm from the source. (*b*) Time of arrival on target versus RC film layer number (data for both active layers A and B of each RC film is plotted).

obtain, in a single shot, information on the temporal history of the object to be probed. In fact, if the object to be probed is situated at a finite distance from the source, protons with different energies will reach the object at different times. By employing a detector that performs spectral selection, the information on the temporal evolution of the target can be retained. This is shown in the plot of figure 5(*b*), where the time of arrival on target of the protons produced on the Al foil is plotted versus the RC film layer number (i.e. versus their energy). As can be seen, the presence of the double active layer in each RC film causes a temporal indetermination which is larger for the first RC layers, but can be removed by mechanically separating the two gel layers after data collection.

In particular, proton imaging was employed to observe the fast evolution of the electric fields following the irradiation of solid targets (wires, foils and micro-balloons) with the CPA_1 pulse. In figure 6 proton images taken (in a single shot) after ultraintense irradiation of a 150 μm glass micro-balloon are shown. The original size and position of the target are indicated by the black circle in figure 6(*c*). Detailed analysis is currently in progress, but some striking features are immediately apparent by simply looking at the data. First of all, in coincidence with the interaction, a shadow, much larger than the target, appears in the image, meaning that the protons are deflected away from the target surface. By matching the deflection to the calculated deflection for protons propagating in a Coulomb field, we could obtain a quantitative measurement of positive whole target charge-up due to the expulsion of fast electrons during the interaction. A rapid discharge was subsequently observed, with a time scale of a few tens of picoseconds.

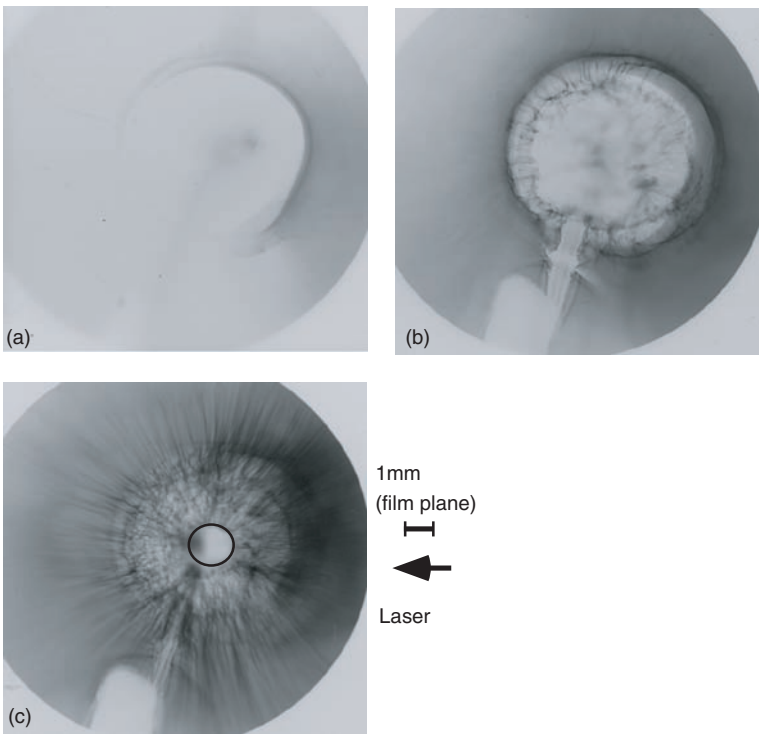

Figure 6. Proton images taken following CPA irradiation of a 150 μm glass micro-balloon. Each picture refers to a different proton energy E_p and a different probing delay Δt from the interaction: (*a*) $E_p \sim 8$ MeV, $\Delta t \sim 0$; (*b*) $E_p \sim 6$–7 MeV, $\Delta t \sim 10$ ps; (*c*) $E_p \sim 3$–5 MeV, $\Delta t \sim 20$–35 ps.

Beside whole target charge-up, other interesting features were seen to develop after the interaction. Among these, the onset of filamentary structures at the target surface after the interaction was observed. The filamentary structures are observed tens of picoseconds after the interaction, and appear as striations extending outwards along the normal to the target surface, even far away from the interaction region. This is clear in figure 6(*b*), where the filaments start to appear, and in figure 6(*c*), where they have fully grown. In figure 6(*c*) the filaments are seen both side-on and face-on (as a speckled pattern inside the shadow). The transverse wavelength of the modulation is of a few tens of microns and is more or less constant over the whole field of observation.

The observations seem to be consistent with the growth, at the surface of the target, of an electromagnetic heat-flow instability [19], such as for example the electro-thermal instability [20]. The instability causes filamentation of the hot current, and as the filaments are magnetized, the effect is imprinted on the proton beam via the radial electric fields present inside the filaments.

7. Conclusions

Proton imaging is a diagnostic with enormous potential for the investigation of fundamental plasma physics problems which were impossible to explore up to now. By using this diagnostic, for the first time the measurement of transient electric fields in dense plasmas has been obtained, determining their evolution on a picosecond scale with micrometric spatial resolution. The data is of great relevance to inertial confinement fusion both in the conventional and fast ignitor approach. While in the simpler configurations, quantitative information can readily be obtained from the data, the interpretation of the most complex structures may require a combination of hydrodynamic, particle-in-cell and particle tracing simulations in order to entangle the field distribution in the plasma. Detailed analysis and modelling is presently ongoing.

Acknowledgments

This work was supported by an ESPRC grant. We acknowledge the invaluable contribution to the work provided by the Central Laser Facility staff at the Rutherford Appleton Laboratory.

References

[1] Clark E L *et al* 2000 *Phys. Rev. Lett.* **84** 670
[2] Snavely R D *et al* 2000 *Phys. Rev. Lett.* **85** 2945
[3] Maksimchuk A *et al* 2000 *Phys. Rev. Lett.* **84** 4108
[4] Gitomer S J *et al* 2000 *Phys. Fluids* **29** 2679
[5] Hatchett S P *et al* 2000 *Phys. Plasmas* **7** 2076
Wilks S *et al* 2001 *Phys. Plasmas* **8** 542
Pukhov A 2001 *Phys. Rev. Lett.* **86** 3562
Ruhl H *et al* 2001 *Plasma Phys. Rep.* **27** 363
[6] Fews P *et al* 1994 *Phys. Rev. Lett.* **73** 1801
Hegelich M *et al 28th European Physical Society Conf. on Controlled Fusion and Plasma Physics*, Book of Abstracts (*Funchal* 2001) ed Silva C, Varandas C, Campbell D, p 717
[7] Clark E L *et al* 2001 *Phys. Rev. Lett.* **85** 1654
[8] Roth M *et al* 2001 *Phys. Rev. Lett.* **86** 436
[9] Koehler A M 1968 *Science* **160** 303
West D, Sherwood A C 1972 *Nature* **239** 157
Cookson J A 1974 *Naturwissenschaften* **61** 184

[10] Schneider U and Pedroni E 1995 *Medical Phys.* **22** 353
Pemler P *et al* 1999 *Nucl. Instr. Methods Phys. Res. A* **432** 483
[11] King N S P *et al* 1999 *Nucl. Instr. Methods Phys. Res. A* **424** 84
[12] Lindl J 1995 *Phys. Plasmas* **2** 3933
[13] Danson C *et al* 1998 *J. Mod. Opt.* **45** 1653
[14] McLaughlin W L C *et al* 1991 *Nucl. Instr. Methods Phys. Res. A* **302**, 165
[15] Enge W 1995 *Radiation Measurements* **25** 11
[16] Mackinnon A J *et al* 2001 *Phys. Rev. Lett.* **86** 1769
[17] Ruhl H *et al* 2001 in preparation
[18] Bett T H *et al* 1995 *Appl. Opt.* **34** 4025
[19] Key M H 1985 *Laser–Plasma Interactions 3*, SUSSP 29
[20] Haines M G 1981 *Phys. Rev. Lett.* **47** 918